

ZU-TH 19/08

QCD CORRECTIONS TO THE RADIATIVE DECAY $B \rightarrow X_s \gamma$

ANDREA FERROGLIA

Institute For Theoretical Physics, University of Zurich, Winterthurerstrasse 190
 Zurich, CH-8057, Switzerland
 andrea.ferrogli@physik.uzh.ch

In this short review, the calculation of the next-to-next-to-leading order QCD corrections to the inclusive radiative decay $B \rightarrow X_s \gamma$ is described. I summarize the salient features of the calculational framework adopted, discuss the results obtained in the last few years, and indicate the technical tools that made the NNLO calculations possible. I conclude by comparing the current NNLO theoretical estimate for the branching ratio with the experimental measurement and by briefly discussing the size and origin of the residual theoretical uncertainty.

Keywords: B meson, inclusive reaction, QCD, radiative correction.

PACS Nos.: 13.20.He, 12.38.Bx.

1. Framework

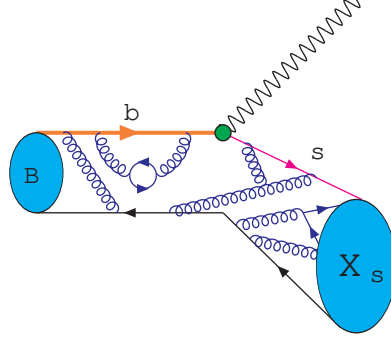
The inclusive radiative decays of B mesons into a photon and an arbitrary hadronic state of total strangeness -1 , $B \rightarrow X_s \gamma$, currently play a relevant role within the precision tests of the Standard Model (SM) and of its extensions. The decay process is sketched in Fig. 1; B denotes a B^- or B^0 mesons, while X_s indicates an inclusive hadronic state not containing charmed particles.

At the parton level, the process in Fig. 1 is induced by a Flavor Changing Neutral Current (FCNC) decay of the b quark contained in the B meson. The b quark decays into a strange quark plus other partons, collectively indicated by the symbol X_s^{parton} , and a photon. In the SM, such a decay takes place at first at one loop, through "penguin" diagrams such as the one shown in Fig. 2. FCNC decays are rare (i.e. loop-suppressed) in the SM; therefore, they are very sensitive to Beyond the SM physics effects, which can arise in the perturbative expansion at the same order as the leading SM contribution.

In contrast with the exclusive decay modes, inclusive decays of B mesons are theoretically clean observables; in fact, it is possible to prove that the decay width $\Gamma(B \rightarrow X_s \gamma)$ is well approximated by the partonic decay rate $\Gamma(b \rightarrow X_s^{\text{parton}} \gamma)$:

$$\Gamma(B \rightarrow X_s \gamma) = \Gamma(b \rightarrow X_s^{\text{parton}} \gamma) + \Gamma_{\text{non-pert}} \quad (1)$$

The second term on the r. h. s. of Eq. (1) represents non-perturbative corrections. The latter are small, since they are suppressed at least by a factor $(\alpha_{\text{QCD}}/m_b)^2$,

Fig. 1. A schematic illustration of the $B \rightarrow X_s$ decay.

where m_b is the b-quark mass and $\alpha_{\text{QCD}} \approx 200 \text{ MeV}$. The relation in Eq. (1) is known as Heavy Quark Expansion (for a review, see Ref. 1).

The partonic process can be studied within the context of perturbative QCD. However, the first-order QCD corrections to the partonic process are very large. The large corrections originate from hard gluon exchanges between quark lines of the one-loop electroweak graphs (see Fig. 3). In general, Feynman diagrams involving different mass scales (say m_1 and m_2 , for example), depend on logarithms of the ratio of the masses. If there is a strong hierarchy among the two mass scales (e.g. $m_1 \gg m_2$), then the logarithms are numerically large. In the case of QCD corrections to the partonic process $b \rightarrow X_s^{\text{parton}}$, the mass scales involved are the W-boson mass M_W , the top quark mass m_t , and m_b . M_W and m_t are of the same order of magnitude $m_W \approx 100 \text{ GeV}$, while the b-quark mass is considerably smaller: $m_b \approx 5 \text{ GeV}$. At n-th order in the perturbative expansion in the strong coupling constant $\alpha_s(m_b)$, one finds terms of the form

$$\alpha_s^n(m_b) \ln^m \frac{m_b}{m_W}; \quad (2)$$

where $m \leq n$. For $n = 1$ and $m = 1$, the product in Eq. (2) is too large to be used as an expansion parameter; terms enhanced by large logarithmic coefficients must be resummed at all orders. Conventionally, calculations performed by resumming logarithms in which $m = n$ are referred to as leading order (LO) precision calculations. By resumming terms in which $m = n-1$, it is possible to obtain results of next-to-leading order (NLO) precision. Similarly, resumming $m = n-1; n-2$ logarithms, it is possible to achieve next-to-next-to-leading order (NNLO) precision.

The easiest way to implement the resummation of the large logarithms discussed above is to work within the context of a renormalization-group-improved effective theory with n_f active quarks. In such a theory, the heavy degrees of freedom involved in the decay under study are integrated out. By means of an operator product expansion, it is possible to factorize the contribution of the short-distance and long-distance dynamics in the decay of the B meson. In the SM, the short-distance dynamic is characterized by mass scales of the order of the top-quark or W-boson mass, while the long-distance dynamic is characterized by the b-quark

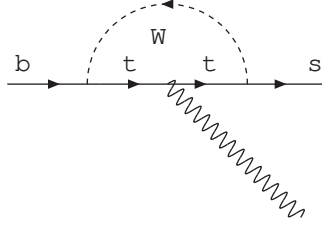


Fig. 2. One of the penguin diagrams contributing to $b \rightarrow s$ decay.

mass. The boundary between short-distance and long-distance is chosen at a low-energy scale μ_b such that $m_b \ll \mu_b \ll M_W$. Clearly, the scale μ_b is unphysical, and therefore physical quantities should not depend on it. However, all calculations are performed up to some fixed order in perturbation theory. This truncation of the perturbative series induces a dependence on the low-energy scale in the physical observables, which is formally of higher order with respect to the precision goal of the calculation. From the practical point of view, the Lagrangian employed in calculating the $b \rightarrow X_s^{\text{parton}}$ decay rate can be written as^a

$$L = L_{\text{QED}} + L_{\text{QCD}}(u,d,c,s,b) + \sum_{i=1}^8 \frac{4G_F}{2} V_{ts} V_{tb} C_i(\mu; m_W) O_i(\mu) + O\left(\frac{m_b}{M_W}\right) \quad (3)$$

In the equation above, L_{QED} and L_{QCD} represent the usual QED and QCD Lagrangians with five active quark flavors. The second term in Eq. (3) is more interesting: G_F is the Fermi constant, V_{ts} and V_{tb} are elements of the CKM matrix, and O_i are eight effective operators of dimensions five and six. Operators with dimensions larger than six are suppressed by inverse powers of the W -boson mass and are ignored. Finally, the short-distance dynamic is encoded in the "coupling constants" of the effective operators, which are called Wilson coefficients and are indicated by C_i in Eq. (3). The Wilson coefficients are the only elements of the Lagrangian which depend on the heavy particles masses M_W and m_t .

Any perturbative calculation of the $b \rightarrow X_s^{\text{parton}}$ decay rate within the context of the renormalization-group-improved perturbation theory applied to the Lagrangian in Eq. (3) requires three different steps:

- i) The first step, conventionally called matching, consists in fixing the value of the Wilson coefficients at the high-energy scale $\mu_w \sim M_W, m_t$. This is achieved by requiring that Green functions calculated in the full SM and in the effective theory provide the same result up to terms suppressed by the ratio between the external momenta and M_W or m_t . At the scale μ_w , QCD corrections are small and subsequently can be calculated in fixed-order perturbation theory.
- ii) Secondly, once the value of the Wilson coefficient at the electroweak scale has been obtained from the matching step, it is then necessary to obtain

^aTerms suppressed by the CKM factor $V_{us} V_{ub}$ are ignored; however, their NLO effect was accounted for in the NNLO calculation of the $B \rightarrow X_s \gamma$ branching ratio in Ref. 2.

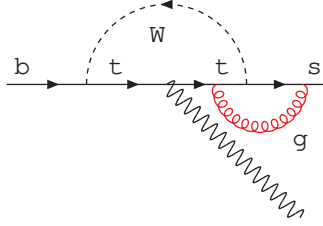


Fig. 3. One of the diagrams contributing to the first order QCD corrections to $b \rightarrow s$ decay.

the value of the Wilson coefficients at the low-energy scale $\mu = m_b$. This can be achieved by solving the system of renormalization group equations (RGE) satisfied by the Wilson coefficient, which have the following form :

$$\frac{d}{d} C_i(\mu) = \gamma_{ji}(\mu) C_j(\mu) : \quad (4)$$

The matrix γ in the equation above is the anomalous dimension matrix (ADM) of the effective operators. Since the various operators mix under renormalization, this step of the calculation is called mixing. By solving the RGE, it is possible to resum at all orders the large logarithms of the ratio $\mu = m_b$ in the Wilson coefficients. This becomes evident by looking at the leading order solution of Eq. (4) (for the diagonalized ADM, indicated by a tilde)

$$C_i(\mu_b) = \left[1 + \frac{\beta_0(\mu_b)}{4} \ln \frac{\mu}{\mu_b} \right]^{-\tilde{\gamma}_{ii}^{(0)}/2\beta_0} C_i(\mu_w) ; \quad (5)$$

where $\beta_0 = 11 - 2/3 N_f$ is the leading order QCD beta function, and N_f is the number of active quarks.

- iii) Finally, it is necessary to calculate on-shell matrix elements of the partonic process in the effective theory. QCD radiative corrections to the matrix elements do not include large logarithms, since the dependence on the heavy degrees of freedom is completely encoded within the Wilson coefficients.

The eight effective operators appearing in the Lagrangian in Eq. (3) are listed in Appendix A. At LO, the $b \rightarrow s$ amplitude is proportional to the effective Wilson coefficient C_7^{eff} ; the effective coefficients were introduced in Ref. 3.

Radiative decays of the B meson were first experimentally observed (in the exclusive $B \rightarrow K$ decay mode) by the CLEO collaboration at Comell in 1993. Nowadays, the branching ratio of the inclusive decay $B \rightarrow X_s$ has been measured by several collaborations. The current world average, obtained by averaging the CLEO, BELLE, and BABAR measurements (Refs. 4, 5, 6, 7, 8), is (Ref. 9)

$$\mathcal{B}(B \rightarrow X_s)_{E > E_0}^{WA} = (3.52 \pm 0.23 \pm 0.09) \cdot 10^4 : \quad (6)$$

In Eq. (6) the first error is due to statistical and systematic uncertainty, while the second is due to theory input on the b-quark Fermi motion. In order to eliminate irreducible backgrounds, experimental collaborations impose a lower cut on the

photon energy. The value in Eq. (6) refers to a lower cut $E_0 = 1.6 \text{ GeV}$. In view of current experimental accuracy, theoretical predictions based upon NLO calculations in the α_s expansion are no longer sufficient. In the last eight years, partial results necessary for the theoretical calculation of the $B \rightarrow X_s \gamma$ branching ratio with NNLO precision were obtained by several groups (Refs. 10, 11, 12, 13, 14, 15, 16, 17, 18, 19, 20, 2). Two years ago, by employing these partial results, it was possible to obtain the first theoretical estimate of the branching ratio at NNLO (2, 21). Currently, the NNLO program is heading toward completion (Ref. 22, 23, 24).

In order to calculate the $B \rightarrow X_s \gamma$ branching ratio at NNLO, it is necessary to make use of some of the most powerful and recent techniques available for multi-loop Feynman diagrams calculations. The aim of the rest of this short review is to indicate the techniques employed in the parts of the NNLO calculation carried out so far, as well as to indicate the areas in which work is currently in progress. I conclude by comparing the current theoretical prediction of the branching ratio with the experimental measurements and by briefly discussing the residual theoretical uncertainties.

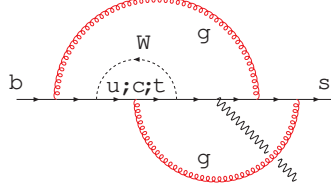
2. NNLO Calculation

The experimental error on the $B \rightarrow X_s \gamma$ branching ratio in Eq. (6) is of 7%. The theoretical error affecting the NLO prediction is about 10% (see for example the comprehensive reviews in Refs. 25, 26). Aside for the NLO QCD corrections (Refs. 27, 28, 29, 30, 31, 32, 33, 34, 35, 36, 37, 38, 39), NLO determinations of the branching ratio include electroweak effects (Refs. 40, 41, 42); moreover, the numerical impact of the charm- and bottom-quark masses was analyzed in detail in Ref. 43. However, the NNLO QCD corrections were estimated to be at the level of

7% already in Ref. 44. The inclusion of the NNLO QCD corrections is expected to significantly reduce the uncertainty associated to the charm-quark mass renormalization scale. In fact, since the charm-quark mass m_c first enters the branching ratio at NLO, the related scale dependence is a NNLO issue (see Ref. 43). It is thus mandatory to include the numerically leading NNLO QCD effects in the theoretical prediction of the $B \rightarrow X_s \gamma$ branching ratio in order to bring the theoretical uncertainty at the same level of the experimental one. Below matching, mixing, and matrix element calculation at NNLO in QCD are discussed.

2.1. Matching

The goal of the matching procedure at NNLO is to calculate the order α_s^2 corrections to the Wilson coefficients evaluated at the high-energy scale $\mu_w = m_t; M_w$. The matching of the four-quark operators $O_1; \dots, O_6$, which requires the calculation of two-loop Feynman diagrams in the SM, was carried out in Ref. 10. Since the magnetic- and chromomagnetic dipole operators O_7 and O_8 first arise at one-loop in the SM, the matching of these operators requires the calculation of three-loop Feynman diagrams, one of which is shown in Fig. 4. The dipole operator matching

Fig. 4. One of approximately 1000 diagrams needed for the NNLO matching of the O_7 operator.

was carried out in Ref. 11. Both Ref. 10 and Ref. 11 employ the same calculational technique. The SM diagrams are expanded in the ratio $(\text{external momenta})^2 = \frac{s}{M_W^2}$ up to the first non-vanishing order. Spurious infrared divergencies originating from the expansion are regulated in dimensional regularization. All the masses, with the exception of M_W , m_t , and m_b , are set equal to zero from the start; terms proportional to m_b^2 are also neglected. The integrals that must be evaluated after the expansion in the external momenta correspond to vacuum diagrams, involving one or, as in Ref. 11, two mass scales. Two- and three-loop vacuum integrals depending on a single mass scale are known. Three-loop vacuum diagrams depending on two different mass scales could not be evaluated directly. The problem was solved by expanding the integrals around the point $m_t = M_W$ and for $m_t \ll M_W$. Both expansions give satisfactory results for the physical value $M_W = m_t = 2$. In order to write down the matching equations, it is necessary to require equivalency of the SM and effective theory Green functions. The calculation of the latter is not problematic; in fact, after expanding in the external momenta, loop diagrams give rise to scaleless integrals, which vanish in dimensional regularization.

2.2. Mixing

The entries of the ADM in Eq. (4) can be obtained from the QCD renormalization constants in the effective theory. The latter are derived from ultraviolet divergencies in the Feynman diagrams with effective operator insertions. The ADM has the following perturbative expansion

$$s^{(k)} = \sum_{k=0}^{\infty} \frac{s^{(k)}}{4} \Gamma^{(k+1)} \Gamma^{(k)}; \quad (7)$$

where the matrices at each order in s have a block structure:

$$\Gamma^{(k)} = \begin{pmatrix} A_{6 \times 6}^{(k)} & B_{6 \times 2}^{(k)} \\ 0_{2 \times 6} & C_{2 \times 2}^{(k)} \end{pmatrix}; \quad (8)$$

The lower-left block vanishes because the dimension-ve dipole operators do not generate UV divergencies in dimension-six, four-quark amplitudes. The matrices $A^{(k)}$ and $C^{(k)}$ can be obtained from the UV divergencies of $(k+1)$ -loop diagrams, while to evaluate $B^{(k)}$ it is necessary to evaluate the UV divergencies of $(k+2)$ -loop diagrams. The matrices $A^{(2)}$, $B^{(2)}$, and $C^{(2)}$ were calculated in the Refs. 12, 14, and 13, respectively. Sample diagrams needed in the calculation of the NNLO ADM are shown in Fig. 5. Since one is interested in Feynman diagrams UV divergencies, it

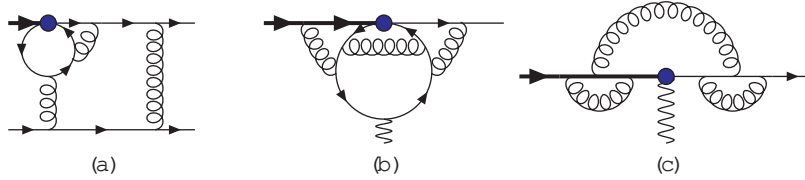


Fig. 5. Examples of Feynman diagrams needed for the calculation of the matrices $A^{(2)}$ (a), $B^{(2)}$ (b), and $C^{(2)}$ (c). Thick arrow lines indicate b quarks, thin arrow lines indicate massless quarks; the dark dots indicate effective operators.

is necessary to evaluate the corresponding integrals by regulating UV and infrared singularities in different ways. In Refs. 12, 14, and 13 this was done by introducing a common mass M for all fields, and thus by expanding the loop integrals in inverse powers of M . Therefore, the only integrals needed were single scale tadpoles up to four loops; these integrals are known. The number of diagrams involved is impressive: the calculation of $B^{(2)}$ alone requires the evaluation of over 20000 four-loop Feynman graphs.

2.3. Matrix Elements – Total Rate

To complete the calculation of the NNLO corrections to the $b \rightarrow X_s^{\text{parton}}$ decay rate, it is necessary to calculate the $O(\alpha_s^2)$ corrections to the matrix elements in the low-energy effective theory of Eq. (3). The decay width for the process $b \rightarrow X_s^{\text{parton}}$ can be written as

$$\Gamma(b \rightarrow X_s^{\text{parton}})_{E > E_0} = \frac{G_F^2 \alpha_{\text{em}} m_b^2 (m_b^3) m_s^3}{32^4} V_{tb} V_{ts}^2 \sum_{ij} C_i^e C_j^e G_{ij}(E_0); \quad (9)$$

The term proportional to G_{ij} in Eq. (9) originates from the interference of diagrams mediated by the effective operator O_i and diagrams involving the effective operator O_j . Consequently, G_{ij} is referred to as the $(O_i; O_j)$ component of the decay width. In Eq. (9) m_b and m_s indicate the pole and running \overline{MS} bottom quark mass, respectively. α_{em} is the fine structure constant at zero momentum transfer. The total decay rate can be obtained from Eq. (9) by setting the lower cut on the photon energy, E_0 , equal to zero. In this section we discuss the calculation of NNLO QCD corrections to the total decay rate.

The $(O_7; O_7)$ component is the only one completely known at NNLO in QCD. This component is numerically dominant and was independently calculated by two different groups (Refs. 16, 17). In order to calculate the NNLO QCD corrections to the $(O_7; O_7)$ component of the decay width in Eq. (9), it is necessary to consider three different sets of matrix elements:

Two-loop corrections to the process $b \rightarrow X_s$ interfered with the tree-level

^bI consider squared amplitudes summed over spin, color, and polarization of the final state, as well as averaged over the spin and color of the incoming b quark.

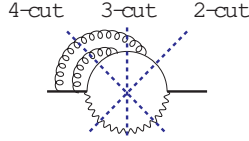


Fig. 6. Two-, three-, and four-particle cuts in a three-loop b-quark self-energy diagram; they all contribute to the $(O_7; O_7)$ component of the NNLO $b \rightarrow s \gamma$ decay rate. Thick lines indicate b quarks, thin lines indicate strange (massless) quarks.

matrix element of the $b \rightarrow s \gamma$ decay, one-loop corrections to the process $b \rightarrow s \gamma$ interfered with the corresponding tree-level amplitude, and tree-level matrix elements for the processes $b \rightarrow s g g$ and $b \rightarrow s q \bar{q}$ interfered among themselves.

The contribution of each of the quantities listed above to the $b \rightarrow s \gamma$ decay width is directly related to the imaginary part of three-loop b-quark self-energy diagrams by means of the optical theorem (an example is shown in Fig. 6). The contribution of each physical cut to the imaginary part of a self-energy can be evaluated by means of the Cutkosky rules (Refs. 45, 46, 47). In Ref. 17, the contribution of each cut of each three-loop b-quark self-energy diagram was evaluated by means of the methods commonly employed in the calculation of multi-loop Feynman diagrams. By employing the Laporta algorithm (Refs. 48, 49, 50, 51), it is possible to rewrite each cut diagram as a linear combination of a small number of Master Integrals (MIs). The Cutkosky rules associate a Dirac delta function with each line going through the cut. The latter sets the momentum flowing through a "cut propagator" on its mass-shell. The delta functions can be written as a difference of propagators (Refs. 52, 53); if q is the momentum flowing through a cut propagator one finds

$$q^2 + m^2 = \frac{1}{2 - i0} \frac{1}{q^2 + m^2 + i0} - \frac{1}{q^2 + m^2 - i0} \quad (10)$$

The reduction procedure is simplified by the fact that all of the integrals in which one of the cut propagators vanishes or is raised to a negative power are equal to zero, since in those cases the $-i0$ prescription in Eq. (10) becomes irrelevant. In Ref. 17, the MIs were evaluated numerically by means of the sector decomposition method (Ref. 54); the four-particle phase space integrals were parameterized according to the methods presented in Refs. 55 and 56. After summing over the contribution of all of the cuts, the residual poles in the dimensional regulator ϵ are canceled by UV renormalization. The methods employed in Ref. 17 can also be applied to the calculation of the $(O_7; O_8)$ and $(O_8; O_8)$ components of the decay width in Eq. (9). The authors of Ref. 16 were able to analytically calculate the $(O_7; O_7)$ component of the $b \rightarrow s \gamma$ decay width. In fact, in Ref. 57, the same authors evaluated the complete imaginary part of individual three-loop b-quark self-energy diagrams. Each imaginary part is the sum of all of the possible cuts present in a given graph. In the case of the $(O_7; O_8)$ and $(O_8; O_8)$ decay width components, not all of the

cuts correspond to the interference of $b \rightarrow X_s \gamma$ matrix elements. Therefore, in order to calculate the $(O_7; O_8)$ and $(O_8; O_8)$ components, it will be necessary to individually evaluate each cut contributing to the process.

The first calculation of $b \rightarrow X_s \gamma$ matrix elements at NNLO was the one described in Ref. 15. In that work, a set of NNLO virtual corrections to the matrix elements involving the effective operators^c O_1, O_2, O_7, O_8 , as well as bremsstrahlung corrections to matrix elements including O_7 , are evaluated. The authors restrict their calculation to diagrams with a closed light-quark loop. In fact, once the correction proportional to $\frac{2}{3}N_1$ (where N_1 is the number of light quarks) are known, it is possible to estimate the complete NNLO corrections by means of the naive non-abelianization hypothesis (NNA, see Refs. 58, 59): the BLM (or large- β_0) approximation is derived by replacing the factor N_1 with the coefficient $\beta_0=2$ in diagrams with a light-quark loop. In Ref. 15, the calculation was carried out by means of Feynman parameterization of the integrands, followed by an integration technique based upon Mellin-Barnes (MB) transform (see Refs. 60, 61, 62). The results are presented in analytic form. The three-loop virtual corrections to the O_1 and O_2 matrix elements are expanded in powers of m_c^2/m_b^2 .

In Ref. 2, Misiak and Steinhauser computed the NNLO corrections in the BLM approximation in the non-physical limit $m_c = m_b=2$. They observed that their result, evaluated at $m_c = m_b=2$, matches well with the calculation of the same set of corrections in the small m_c expansion (Ref. 15). Because of this match, Misiak and Steinhauser also evaluated the complete m_c -dependent NNLO corrections to the $b \rightarrow X_s \gamma$ matrix elements in the $m_c = m_b=2$ approximation. Subsequently, they assumed that the BLM result is a good approximation of the full NNLO corrections for $m_c = 0$, and they interpolated their results for the non-BLM corrections down to the measured value of m_c . The calculational technique employed in Ref. 2 is the same technique employed in the three-loop Wilson coefficient calculation presented in Ref. 11. The results of Refs. 15 and 2 were crucial to obtain the first NNLO estimate of the $B \rightarrow X_s \gamma$ branching ratio (Refs. 2, 21). However, the calculation of the NNLO QCD corrections to the $b \rightarrow X_s \gamma$ matrix elements is not yet complete, and several groups are still working to improve the understanding of this set of corrections.

In Ref. 24, the authors reconsider the virtual fermion loop corrections to the matrix elements involving the operators O_1 and O_2 . They check the result of Ref. 15 by evaluating the corrections proportional to $\frac{2}{3}N_1$, and they also numerically calculate the diagrams involving a closed massive charm or bottom quark loop. In the case of diagrams involving massless quark loops the reduction is carried out by means of the Laporta algorithm, while the MIs are evaluated in two different ways; first in an expansion in powers of m_c/m_b , and then by the numerical evaluation of the

^cAt NNLO it is possible to neglect the operators $O_3; \dots; O_6$, since they are suppressed by small Wilson coefficients; the NLO contribution to the branching ratio arising from these operators is $< 1\%$.

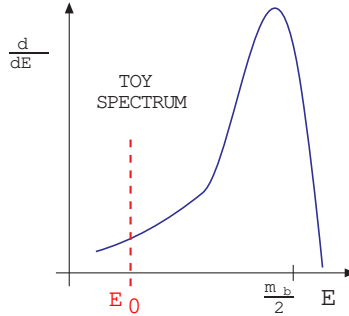


Fig. 7. A sketch of the photon energy spectrum in the $B \rightarrow X_s$ decay. Only photons with energy $E > E_0$ are observed.

MB representation of the integrals. The Laporta algorithm is also employed for diagrams involving a massive quark loop. However, for some of the MIs encountered in the latter case, the numerical evaluation of MB representations is not sufficiently precise. In these cases, an interesting technique based upon the numerical solution of the system of differential equations satisfied by the MIs is adopted.

The effects of the charm-quark mass in the $(O_7; O_7)$ and $(O_7; O_8)$ decay width components are analyzed in Ref. 22 and Ref. 23.

Currently, a group is working on the numerical calculation of the $(O_1; O_7)$ and $(O_2; O_7)$ components in the $m_c = 0$ approximation (Refs. 63, 64). The latter represents the first step toward the calculation of the complete set of NNLO corrections in the $m_c = 0$ limit. Once this result becomes available, it will then be possible to interpolate the results of Ref. 2 to the physical value of m_c without making any assumption on the behavior of the corrections for vanishing m_c . In turn, this procedure will reduce the error associated with the m_c interpolation.

2.4. Matrix Elements – Spectrum

In the two-body $b \rightarrow s$ decay, the energy of the outgoing photon is fixed by the kinematic of the process: $E = m_b/2$ in the b -quark rest frame. However, two different phenomena give rise to a photon energy spectrum in the $B \rightarrow X_s$ decay. First, the partonic decay in which one is interested is not $b \rightarrow s$ but rather $b \rightarrow X_s^{\text{parton}}$; in events involving the emission of one or more gluon or $q\bar{q}$ pair, the photon has an energy $E < m_b/2$. Secondly, the Fermi motion of the b quark in the B meson also contributes in generating a non-trivial photon energy spectrum. The situation is sketched in Fig 7; the smearing of the photon energy spectrum beyond the partonic endpoint $m_b/2$ is due to the non-perturbative Fermi motion effects, while the long low-energy tail has its origin in the gluon/quark-pair bremsstrahlung. The latter can be studied in perturbative QCD, while Fermi motion effects are modeled by means of a process-independent shape function (see Ref. 44, 65). Since experimental collaborations apply a lower cut on the photon energy of about $1.8 - 2 \text{ GeV}$, a detailed knowledge of the photon energy spectrum is mandatory in order to obtain a prediction for the $B \rightarrow X_s$ branching ratio. The measured photon energy spectrum

provides direct information on the shape function, while from the moments of the truncated spectrum it is possible to extract relevant information on the Heavy Quark Expansion parameters.

Working at NLO in α_s , it is necessary to consider the virtual corrections to the process $b \rightarrow s \gamma$ together with the matrix elements of the corresponding process with a gluon in the final state: $b \rightarrow s g$. At NNLO, it is also necessary to consider the matrix elements with up to two gluons or a $q\bar{q}$ pair in the final state. After defining the dimensionless variable $z = 2E_\gamma/m_b$ ($0 \leq z \leq 1$), the quantity G_{ij} in Eq. (9) can be written as

$$G_{ij}(E_\gamma; m_b) = \int_{z_0}^1 \frac{dG_{ij}(z)}{dz} dz; \quad (11)$$

where one sets $z_0 = 2E_\gamma/m_b$ and $z = m_b$, and $dG_{ij} = dz$ is the photon energy spectrum.

The only component of the photon energy spectrum completely known at NNLO in QCD is G_{77} (Refs. 19, 20), which originates from the interference of graphs involving the magnetic dipole operator O_7 . This component of the spectrum is the numerically dominant one. The general structure of a spectrum component $(O_i; O_j)$ is the following:

$$\frac{dG_{ij}(z)}{dz} = f_{ij}(1-z) + R_{ij}(z); \quad (12)$$

Because of kinematics, only matrix elements with three or four particles in the final state contribute to the function $R(z)$. Therefore, if the total decay rate $G_{ij}(z_0 = 0)$ is known, it is sufficient to calculate the function $R(z)$ in Eq. (12), keeping $z \ll 1$, in order to know the photon energy spectrum. The constant f in Eq. (12) can be fixed a posteriori by requiring the equality of the total rate with the integral in Eq. (11) once one sets $z_0 = 0$. The $(O_7; O_7)$ component of the total decay rate can be found in Refs. 16 and 17. Consequently, in order to calculate the corresponding spectrum component, it is sufficient to consider one-loop corrections to the process $b \rightarrow s g$, as well as tree-level matrix elements contributing to the processes $b \rightarrow s g g$ and $b \rightarrow s q\bar{q}$. At NLO, there are just two Feynman diagrams contributing to the $(O_7; O_7)$ spectrum for $z \ll 1$. The squared amplitudes of the two graphs must be integrated over the final-state phase space, and the integrand must be multiplied by a Dirac delta function fixing the energy of the photon. Schematically,

$$\frac{dG_{77}(z)}{dz} \Big|_{\text{NLO}} = \int_{\text{phase space}} \left[\text{Diagram 1} + \text{Diagram 2} \right] \delta(z - \frac{2E_\gamma}{m_b}); \quad (13)$$

The optical theorem relates the decay width to the imaginary part of two-loop b -quarks self-energy diagrams. The contribution of each specific physical cut to the imaginary part of the two-loop self-energy diagrams can be calculated by means of the Cutkosky rules. In particular, the quantity in Eq. (13) is obtained by summing

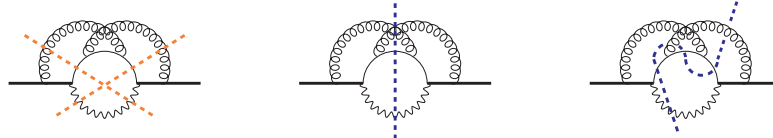


Fig. 8. Cuts contributing to the $b \rightarrow sg$, $b \rightarrow gg$, and $b \rightarrow sss$ processes in a three-loop b -quark self-energy diagram.

over three different cut diagrams

$$\frac{dG_{77}(z)}{dz} \Big|_{\text{NLO}} = \text{[Diagram 1]} + \text{[Diagram 2]} + \text{[Diagram 3]} ; \quad (14)$$

where it is understood that the Dirac delta in Eq. (13) was inserted by hand in the integrands. The same principle can be applied at NNLO, so that the $(O_7; O_7)$ photon energy spectrum can be obtained by calculating appropriate cuts of three-loop b -quark self-energy diagrams; examples are shown in Fig. 8. The contribution of each cut to the photon energy spectrum can be evaluated with the techniques discussed in the previous section. The Dirac delta function employed in order to fix the photon energy can be rewritten as a difference of propagators by means of the identity in Eq. (10) already employed for the delta functions associated with cut propagators. The MIs can then be calculated in different ways. The differential equation method (Refs. 66, 67) was employed in both Ref. 19 and Ref. 20. In Ref. 20, all of the MIs were checked numerically by means of the sector decomposition method. The sum of all of the cuts contributing to the magnetic dipole component of the spectrum is free from collinear and soft divergencies. In the intermediate stages of the calculation, the latter are regulated by dimensional regularization. The residual single pole in the dimensional regulator ϵ is canceled by ultraviolet renormalization. The $(O_7; O_7)$ spectrum is singular in the $z \rightarrow 1$ limit; the singularities appear in the spectrum as plus distributions of the form $[\ln^n(1-z)]_+ = (1-z)_+^{-n}$ ($n = 0, \dots, 3$). The singular terms were also predicted on the basis of the universality of soft and collinear gluon radiation (Ref. 68). It is interesting to observe that in the $z \rightarrow 0$ limit the $(O_7; O_7)$ component of the spectrum should vanish like z^3 . This can be easily proved; each effective operator O_7 gives rise to a factor z in the spectrum, and an additional factor z originates from the integration over the photon phase space. In a similar way, it is possible to determine the behavior of other components of the spectrum in the $z \rightarrow 0$ limit. Since the QED coupling of the quarks with the photon is proportional to $1/E$ for soft photons, the $(O_7; O_8)$ component of the photon energy spectrum is proportional to z when $z \rightarrow 0$. In the same limit, the $(O_8; O_8)$ component of the spectrum behaves like $1-z$. These kinds of considerations are based upon the Feynman rules employed in the calculation; therefore, they apply to each cut of each diagram contributing to a given spectrum component. The qualitative information on the spectrum behavior in the $z \rightarrow 0$ limit can be used as a powerful check of the calculation, but it can also be employed to fix some of the initial conditions needed to calculate the MIs with the differential equation method. In Refs. 16 and 17 the

c-quark mass is set to zero. The exact dependence of the NNLO corrections to the $(O_7; O_7)$ spectrum and total decay rate on the c-quark mass is found in Ref. 22.

The techniques outlined above can in principle be used to also calculate the NNLO QCD corrections to the $(O_7; O_8)$ component of the spectrum. In particular, the dependence of the $(O_7; O_8)$ spectrum on the c-quark mass was studied in Ref. 23.

The BLM corrections to all of the components of the photon energy spectrum, with the exception of $(O_8; O_8)$, were calculated almost a decade ago (see Ref. 18). It is well known that the BLM corrections, which are proportional to $\frac{2}{s} \alpha_s$, usually provide a reliable estimate of the full $\frac{2}{s} \alpha_s$ corrections. In the case of the $(O_7; O_7)$ spectrum component it was possible to verify that the BLM approximation provides a good estimate of the complete NNLO corrections. The BLM corrections to the $(O_8; O_8)$ spectrum component were not calculated in Ref. 18; they are suppressed by a factor $(Q_d C_8 = C_7)^2 \approx 0.03$, and therefore they are expected to be numerically small. Moreover, the $(O_8; O_8)$ spectrum component includes logarithmic singularities in the limit in which the strange quark is considered massless. As discussed above, the $(O_8; O_8)$ spectrum is also singular in the limit of vanishing photon energy; therefore, its contribution to the branching ratio becomes numerically large for low (and experimentally unattainable) values of the cut on the photon energy. For completeness, the BLM corrections to the $(O_8; O_8)$ spectrum were recently computed in Ref. 69; the collinear singularities were regulated by keeping a finite strange quark mass m_s when needed.

Finally, Table 1 summarizes the available NNLO QCD corrections to the matrix elements of the $b \rightarrow X_s^{\text{parton}}$ decay width, indicating both calculations of the total decay rate and of the photon energy spectrum.

Table 1. NNLO QCD corrections to the various component of the $b \rightarrow X_s^{\text{parton}}$ decay width. The first row of the table refers to the full $\frac{2}{s} \alpha_s$ corrections, the second refers to the $\frac{2}{s} \alpha_s$ corrections with a light-quark loop, the third to $\frac{2}{s} \alpha_s$ corrections with a massive charm- or bottom-quark loop, and the fourth to non-BLM corrections in the $m_c = m_b = 2$ approximation.

App.	$(O_1; O_1)$ $(O_1; O_2)$ $(O_2; O_2)$	$(O_1; O_7)$ $(O_2; O_7)$	$(O_1; O_8)$ $(O_2; O_8)$	$(O_7; O_7)$	$(O_7; O_8)$ $(O_8; O_8)$
full $\frac{2}{s} \alpha_s$				Refs. 16, 17, 19, 20	
$\frac{2}{s} N_1$	Ref. 18	Refs. 18, 15, 24		Refs. 18, 15	Refs. 18, 15, 69
c-b loops		Ref. 24		Ref. 22	Refs. 23, 69
$m_c = m_b = 2$	Ref. 2	Ref. 2	Ref. 2	Ref. 2	

3. NNLO Estimate of the B Branching Ratio

According to the procedure of Ref. 43, which is designed in order to reduce parametric uncertainties originating from CKM angles and c- and b-quark masses, the

$B \rightarrow X_s$ branching ratio can be written as

$$\mathcal{B}(B \rightarrow X_s)_{E > E_0} = \mathcal{B}(B \rightarrow X_{ce}) \exp \left[\frac{V_{ts} V_{tb}}{V_{cb}} \frac{\alpha_s^2}{C} [P(E_0) + N(E_0)] \right]; \quad (15)$$

where the perturbative corrections $P(E_0)$ are defined as follows

$$\frac{V_{ts} V_{tb}}{V_{cb}} \frac{\alpha_s^2}{C} P(E_0) = \frac{V_{ub}^2}{V_{cb}} \frac{(\mathcal{B}(X_s^{\text{parton}})_{E > E_0})}{(\mathcal{B}(X_{ue})_{E > E_0})}; \quad (16)$$

and $N(E_0)$ denotes non-perturbative corrections. The factor C is given by

$$C = \frac{V_{ub}^2}{V_{cb}} \frac{\mathcal{B}(X_{ce})}{\mathcal{B}(X_{ue})}; \quad (17)$$

Since C is a ratio of inclusive decay widths, it can be calculated by means of the same tools employed in the calculation of the $B \rightarrow X_s$ width, and expressed as a double series in powers of α_s and of α_{QCD}/m_b (see Ref. 70 for a recent analysis).

The current theoretical estimate of the quantity in Eq. (15) in the SM is (Refs. 2, 21)

$$\mathcal{B}(B \rightarrow X_s)_{E > 1.6 \text{ GeV}}^{\text{SM}} = (3.15 \pm 0.23) \cdot 10^4; \quad (18)$$

The estimate in Eq. (18) includes all of the numerically leading NNLO QCD corrections. When the value of C obtained in Ref. 70 is employed, the central value of Eq. (18) increases by a few percent. The error on the theoretical estimate is about 7%, and was obtained by combining in quadrature four different uncertainties: parametric uncertainty (3%), uncertainty due to missing higher order corrections (3%), uncertainty due to non-perturbative corrections (5%), and uncertainty due to the m_c -interpolation ambiguity of Ref. 2 (3%). The estimate of Eq. (18) does not include some NNLO and non-perturbative corrections which are currently known; however, the combined effect of the neglected contributions is about +1.6%, which is a small correction compared to the theoretical uncertainty (more details can be found in Ref. 71). It is important to observe that the result of Refs. 2, 21 reduced the theoretical uncertainty, which is approximately of the same magnitude as the experimental one. As expected, the inclusion of NNLO corrections significantly reduced the dependence of the branching ratio on the matching scale $\mu_w = M_w$, on the low-energy scale $\mu_b = m_b$, and especially on the charm-mass \overline{MS} renormalization scale μ_c that first enters the calculation at NLO. The scale dependence of the LO, NLO, and NNLO predictions for the branching ratio are compared in Fig. 2 of Ref. 21. The SM theoretical prediction of Eq. (18) is now slightly more than 1% lower than the experimental average in Eq. (6). Such an agreement can be used in order to set stringent constraints on the parameters of some Beyond the SM physics models (see for example Ref. 21).

While progress in the calculation of perturbative corrections to the $b \rightarrow X_s^{\text{parton}}$ decay width is expected in the future, the current theoretical error is dominated by the uncertainty associated to non-perturbative effects, estimated to be about

5% (Ref. 21). The non-perturbative uncertainty primarily arises from corrections of order $O(\alpha_s^2)$ which are very difficult to evaluate; they were analyzed in Ref. 72.

In Table 2, I summarize the size of NLO, NNLO, and non-perturbative corrections to the branching ratio.

Table 2. Size of various perturbative and non-perturbative set of corrections to $B(B \rightarrow X_s \gamma)_{E > 1.6 \text{ GeV}}^{SM}$. The percentages refer to the size of a given set of corrections with respect to a LO branching ratio of $3.4 \cdot 10^{-4}$. The corrections of $O(\alpha_s^2)$ are not yet known.

Perturbative		Non-perturbative	
NLO QCD $O(\alpha_s)$	30%	LO QCD + NLO $m_b O(\frac{2}{QCD} = m_b^2)$	1%
NLO EW $O(\alpha)$	4%	LO QCD + NLO $m_c O(\frac{2}{QCD} = m_c^2)$	3%
NNLO QCD $O(\alpha_s^2)$	10%	NLO QCD + NLO $m_b O(\alpha_s^2)$	5%

In conclusion, the program which aims to calculate the NNLO QCD corrections to the $b \rightarrow X_s^{\text{parton}}$ decay is well underway. The results so far obtained already have a substantial impact on the theoretical prediction of the $B \rightarrow X_s \gamma$ SM branching ratio. The calculation of the NNLO corrections poses numerous technical challenges related to the number of Feynman diagrams involved in various steps of the calculation, as well as to the evaluation of the needed integrals. Such challenges require the extensive application of the most current calculational techniques developed for the automated evaluation of multi-loop Feynman diagrams.

Appendix A. Effective Operators

For completeness, the eight effective operators relevant for the $b \rightarrow X_s^{\text{parton}}$ decay are listed below:

$$\begin{aligned}
 O_1 &= (s \gamma^\mu T^a P_L c) (c \gamma_\mu T^a P_L b) ; \\
 O_2 &= (s \gamma^\mu P_L c) (c \gamma_\mu P_L b) ; \\
 O_3 &= (s \gamma^\mu P_L b) (\bar{q} \gamma_\mu q) ; \\
 O_4 &= (s \gamma^\mu T^a P_L b) (\bar{q} \gamma_\mu T^a q) ; \\
 O_5 &= (s \gamma^\mu P_L b) (\bar{q} \gamma_\mu q) ; \\
 O_6 &= (s \gamma^\mu T^a P_L b) (\bar{q} \gamma_\mu T^a q) ; \\
 O_7 &= \frac{e}{16} m_b (s \gamma^\mu P_R b) F_\mu ; \\
 O_8 &= \frac{g_s}{16} m_b (s \gamma^\mu T^a P_R b) G_\mu^a ; \tag{A.1}
 \end{aligned}$$

In the above equations, e and F (g_s and G) represent the electromagnetic (strong) coupling constant and field strength, respectively. The eight color generators are indicated by T^a . The sums in the operators $O_3; \dots; O_6$ run over the light quarks.

Acknowledgments

I would like to thank P. Gambino for a number of discussions and suggestions, and K. Varade for a careful reading of the manuscript. I am grateful to U. Haisch for several interesting discussions and for providing the numbers in Table 2. This work was supported by the Swiss National Science Foundation (SNF) under contract 200020-117602.

References

1. A. V. Manohar and M. B. Wise, *Camb. Monogr. Part. Phys. Nucl. Phys. Cosmol.* 10 1 (2000).
2. M. Misiak and M. Steinhauser, *Nucl. Phys. B* 764, 62 (2007) [[arXiv:hep-ph/0609241](#)].
3. A. J. Buras, M. Misiak, M. Munz and S. Pokorski, *Nucl. Phys. B* 424, 374 (1994) [[arXiv:hep-ph/9311345](#)].
4. S. Chen et al. [CLEO Collaboration], *Phys. Rev. Lett.* 87, 251807 (2001) [[arXiv:hep-ex/0108032](#)].
5. K. Abe et al. [Belle Collaboration], *Phys. Lett. B* 511, 151 (2001) [[arXiv:hep-ex/0103042](#)].
6. B. Aubert et al. [BABAR Collaboration], *Phys. Rev. D* 72, 052004 (2005) [[arXiv:hep-ex/0508004](#)].
7. B. Aubert et al. [BaBar Collaboration], *Phys. Rev. Lett.* 97, 171803 (2006) [[arXiv:hep-ex/0607071](#)].
8. B. Aubert et al. [BaBar Collaboration], *Phys. Rev. Lett.* 97, 171803 (2006) [[arXiv:hep-ex/0607071](#)].
9. E. Barberio et al., [arXiv:0808.1297 \[hep-ex\]](#).
10. C. Bobeth, M. Misiak and J. Urban, *Nucl. Phys. B* 567, 153 (2000) [[arXiv:hep-ph/9904413](#)].
11. M. Misiak and M. Steinhauser, *Nucl. Phys. B* 683, 277 (2004) [[arXiv:hep-ph/0401041](#)].
12. M. Gorbahn and U. Haisch, *Nucl. Phys. B* 713, 291 (2005) [[arXiv:hep-ph/0411071](#)].
13. M. Gorbahn, U. Haisch and M. Misiak, *Phys. Rev. Lett.* 95, 102004 (2005) [[arXiv:hep-ph/0504194](#)].
14. M. Czakon, U. Haisch and M. Misiak, *JHEP* 0703, 008 (2007) [[arXiv:hep-ph/0612329](#)].
15. K. Bieri, C. Greub and M. Steinhauser, *Phys. Rev. D* 67, 114019 (2003) [[arXiv:hep-ph/0302051](#)].
16. I. R. Blokland, A. Czarnecki, M. Misiak, M. Slusarczyk and F. Tkachov, *Phys. Rev. D* 72, 033014 (2005) [[arXiv:hep-ph/0506055](#)].
17. H. M. Asatrian, A. Hovhannisyian, V. Poghosyan, T. Ewerth, C. Greub and T. Hurth, *Nucl. Phys. B* 749, 325 (2006) [[arXiv:hep-ph/0605009](#)].
18. Z. Ligeti, M. E. Luke, A. V. Manohar and M. B. Wise, *Phys. Rev. D* 60, 034019 (1999) [[arXiv:hep-ph/9903305](#)].
19. K. Melnikov and A. Mitov, *Phys. Lett. B* 620, 69 (2005) [[arXiv:hep-ph/0505097](#)].
20. H. M. Asatrian, T. Ewerth, A. FerrogliA, P. Gambino and C. Greub, *Nucl. Phys. B* 762, 212 (2007) [[arXiv:hep-ph/0607316](#)].

21. M. Misiak et al., Phys. Rev. Lett. 98, 022002 (2007) [arXiv:hep-ph/0609232].
22. H. M. Asatrian, T. Ewerth, H. Gabrielyan and C. Greub, Phys. Lett. B 647, 173 (2007) [arXiv:hep-ph/0611123].
23. T. Ewerth, arXiv:0805.3911 [hep-ph].
24. R. Boughezal, M. Czakon and T. Schutzmeier, JHEP 0709, 072 (2007) [arXiv:0707.3090 [hep-ph]].
25. A. J. Buras and M. Misiak, Acta Phys. Polon. B 33, 2597 (2002) [arXiv:hep-ph/0207131].
26. T. Hurth, Rev. Mod. Phys. 75, 1159 (2003) [arXiv:hep-ph/0212304].
27. K. Adel and Y. P. Yao, Phys. Rev. D 49, 4945 (1994) [arXiv:hep-ph/9308349].
28. C. Greub and T. Hurth, Phys. Rev. D 56, 2934 (1997) [arXiv:hep-ph/9703349].
29. M. Ciuchini, G. Degrassi, P. Gambino and G. F. Giudice, Nucl. Phys. B 527, 21 (1998) [arXiv:hep-ph/9710335].
30. A. J. Buras, A. Kwiatkowski and N. Pott, Nucl. Phys. B 517, 353 (1998) [arXiv:hep-ph/9710336].
31. K. G. Chetyrkin, M. Misiak and M. Munz, Phys. Lett. B 400, 206 (1997) [Erratum - ibid. B 425, 414 (1998)] [arXiv:hep-ph/9612313].
32. P. Gambino, M. Gorbahn and U. Haisch, Nucl. Phys. B 673, 238 (2003) [arXiv:hep-ph/0306079].
33. A. Ali and C. Greub, Z. Phys. C 49, 431 (1991).
34. A. Ali and C. Greub, Phys. Lett. B 361, 146 (1995) [arXiv:hep-ph/9506374].
35. N. Pott, Phys. Rev. D 54, 938 (1996) [arXiv:hep-ph/9512252].
36. C. Greub, T. Hurth and D. Wyler, Phys. Lett. B 380, 385 (1996) [arXiv:hep-ph/9602281].
37. C. Greub, T. Hurth and D. Wyler, Phys. Rev. D 54, 3350 (1996) [arXiv:hep-ph/9603404].
38. A. J. Buras, A. Czamecki, M. Misiak and J. Urban, Nucl. Phys. B 611, 488 (2001) [arXiv:hep-ph/0105160].
39. A. J. Buras, A. Czamecki, M. Misiak and J. Urban, Nucl. Phys. B 631, 219 (2002) [arXiv:hep-ph/0203135].
40. A. Czamecki and W. J. Marciano, Phys. Rev. Lett. 81, 277 (1998) [arXiv:hep-ph/9804252].
41. K. Baranowski and M. Misiak, Phys. Lett. B 483, 410 (2000) [arXiv:hep-ph/9907427].
42. P. Gambino and U. Haisch, JHEP 0009, 001 (2000) [arXiv:hep-ph/0007259].
43. P. Gambino and M. Misiak, Nucl. Phys. B 611, 338 (2001) [arXiv:hep-ph/0104034].
44. A. L. Kagan and M. Neubert, Eur. Phys. J. C 7, 5 (1999) [arXiv:hep-ph/9805303].
45. R. E. Cutkosky, J. Math. Phys. 1, 429 (1960).
46. M. J. G. Velthuis, Physica 29, 186 (1963).
47. E. Remiddi, Helv. Phys. Acta 54, 364 (1982).
48. S. Laporta and E. Remiddi, Phys. Lett. B 379, 283 (1996) [arXiv:hep-ph/9602417].
49. S. Laporta, Int. J. Mod. Phys. A 15, 5087 (2000) [arXiv:hep-ph/0102033].
50. F. V. Tkachov, Phys. Lett. B 100, 65 (1981).
51. K. G. Chetyrkin and F. V. Tkachov, Nucl. Phys. B 192, 159 (1981).
52. C. Anastasiou and K. Melnikov, Nucl. Phys. B 646, 220 (2002) [arXiv:hep-ph/0207004].
53. C. Anastasiou, L. J. Dixon, K. Melnikov and F. Petriello, Phys. Rev. D 69, 094008 (2004) [arXiv:hep-ph/0312266].
54. T. Binoth and G. Heinrich, Nucl. Phys. B 680, 375 (2004) [arXiv:hep-ph/0305234].
55. C. Anastasiou, K. Melnikov and F. Petriello, Phys. Rev. D 69, 076010 (2004) [arXiv:hep-ph/0311311].

56. A . G ehmann-D e R idder, T . G ehmann and G . H einrich, Nucl. Phys. B 682, 265 (2004) [arX iv:hep-ph/0311276].
57. I. R . B lokland, A . C zamecki, M . S lusarczyk and F . T kachov, Phys. Rev. D 71, 054004 (2005) [arX iv:hep-ph/0503039].
58. S . J . B rodsky, G . P . L epage and P . B . M ackenzie, Phys. Rev. D 28, 228 (1983).
59. M . B eneke and V . M . B raun, Phys. Lett. B 348, 513 (1995) [arX iv:hep-ph/9411229].
60. V . A . S m imov, Phys. Lett. B 460, 397 (1999) [arX iv:hep-ph/9905323].
61. J . B . T ausk, Phys. Lett. B 469, 225 (1999) [arX iv:hep-ph/9909506].
62. V . A . S m imov, "Feynman integral calculus," Berlin, G erm any: Springer (2006) 283 p
63. R . B oughezal, arX iv:0712.1676 [hep-ph].
64. T . S chutzmeier, arX iv:0807.0915 [hep-ph].
65. Z . L igeti, I. W . S tewart and F . J . T ackmann, arX iv:0807.1926 [hep-ph].
66. E . R em idi, Nuovo C in . A 110, 1435 (1997) [arX iv:hep-th/9711188].
67. M . A rgeri and P . M astrolia, Int. J. M od. Phys. A 22, 4375 (2007) [arX iv:0707.4037 [hep-ph]].
68. J . R . A ndersen and E . G ardi, JHEP 0506, 030 (2005) [arX iv:hep-ph/0502159].
69. A . F errogliA and U . H aisch, in preparation.
70. P . G ambino and P . G iordano, arX iv:0805.0271 [hep-ph].
71. M . M isiak, arX iv:0808.3134 [hep-ph].
72. S . J . L ee, M . N eubert and G . P az, Phys. Rev. D 75, 114005 (2007) [arX iv:hep-ph/0609224].